
Assessment and Comparison of Three Scatter Correction Techniques in Single Photon Emission Computed Tomography

Maria Carla Gilardi, Valentino Bettinardi, Andrew Todd-Pokropek, Luciano Milanese, and Ferruccio Fazio

ITBA, CNR Milano; Istituto S. Raffaele, Milano; University College London, London, England; Dipartimento di Scienze e Tecnologie Biomediche, University of Milano, Italy

The detection of scattered radiation is recognized as one of the major sources of error in single photon emission computed tomography (SPECT). In this work three scatter correction techniques have been assessed and compared. Scatter coefficients and parameters characteristic of each technique have been calculated through Monte Carlo simulations and experimentally measured for various source geometries. Their dependence on the source/matter distribution and their spatial non-stationarity have been described. Each of the three scatter correction methods has then been tested on several SPECT phantom studies. The three methods provided comparable results. Following scatter compensation, both image quality and quantitative accuracy improved. In particular a slight improvement in spatial resolution and a statistically significant increase in cold lesion contrast, hot lesion recovery coefficient, and signal/noise ratio have been demonstrated with all methods.

J Nucl Med 29:1971-1979, 1988

The detection of scattered radiation is one of the major sources of error in single photon emission computed tomography (SPECT). When a photon is scattered following a Compton effect it loses its original energy and direction. Degradation in energy can be used to identify scattered photons and to eliminate them from detection, by setting an appropriate energy window with the lower threshold very close to the energy of primary photons (photopeak window). In most of the commercially-available SPECT systems, NaI(Tl) crystals are used as detectors; this scintillator has a poor energy resolution (12% at 140 keV) and a scatter component is included within the photopeak energy window. Being impossible to distinguish and thus eliminate this scatter contribution during acquisition, several scatter correction procedures have been proposed, in order to improve image quality and to provide quantitative results in SPECT (1-8). The aim of this work was to evaluate the convolution subtraction method suggested by Axelsson et al. (1) and two multiple energy windows methods as proposed by Jaszczak

et al. (2) and Todd-Pokropek et al. (3). All three methods are based on the subtraction of a Compton component from the photopeak data, but differ in estimating the Compton component itself.

This work consists of two parts: the assessment of the three scatter correction techniques by estimating scatter coefficients and parameters through Monte Carlo simulations and experimental measurements, and the comparison of the methods on the basis of technetium-99m (^{99m}Tc) SPECT experimental studies.

METHODS

Convolution Subtraction Method of Scatter Correction

In the convolution subtraction method proposed by Axelsson et al. (1), the scatter component within the photopeak window, $S(x, \Phi)$, at position x and angle Φ , is calculated as a convolution (\bullet) of the measured photopeak projection, $P(x, \Phi)$, with a scatter distribution function $f(x)$

$$S(x, \Phi) = P(x, \Phi) \bullet f(x). \quad (1)$$

$f(x)$ is a function characteristic of the individual tomographic system, and may be modeled as a monoexponential function, $f(x) = A \exp(-Bx)$, where the constants A and B are derived from the measurement of line spread functions (LSF) in a

Received Oct. 7, 1987; revision accepted May 19, 1988.

For reprints contact: Maria Carla Gilardi, ITBA CNR, via Olgettina 60, 20132 Milano, Italy.

scattering medium. The scatter corrected projections, $T(x, \Phi)$, are obtained from

$$T(x, \Phi) = P(x, \Phi) - S(x, \Phi) \quad (2)$$

Dual Energy Window Method of Scatter Correction

In the dual energy window acquisition technique, proposed by Jaszczak et al. (2), tomographic data are simultaneously recorded within the primary photopeak energy window (e.g. 140 keV, 20% for ^{99m}Tc) and within a secondary lower Compton window (e.g., 92–125 keV). The scatter compensation consists of the subtraction of a fraction K_J of the Compton reconstructed image, $C(x, y)$, from the photopeak tomogram $P(x, y)$

$$S(x, y) = K_J \cdot C(x, y) \quad (3)$$

$$T(x, y) = P(x, y) - S(x, y), \quad (4)$$

where $S(x, y)$ represents the scatter component within the photopeak energy window and $T(x, y)$ is the scatter compensated image. A value of $K_J = 0.5$ was proposed, based on both Monte Carlo simulations and experimental measurements. Considering that both the reconstruction backprojection algorithm and the scatter compensation procedures are linear, scatter correction can be equally performed before or after image reconstruction. The "projection version" of the method was implemented here, by performing the weighted subtraction directly on projections, before the reconstruction.

Multi-Energy Window—Filtering Method of Scatter Correction

A multi-energy window acquisition technique has been proposed by Todd-Pokropek et al. (3). By this method the scatter component within the photopeak energy window is calculated as a weighted mean of contributions from data recorded within different Compton windows. As the system has different transfer functions at different energy windows, Compton projections must be convolved with appropriate filter functions

$$S(x, \Phi) = \sum_i K_{Ti} \cdot C_i(x, \Phi) \bullet h_i(x), \quad (5)$$

where $S(x, \Phi)$ is the calculated scatter photopeak projection, $C_i(x, \Phi)$, K_{Ti} , $h_i(x)$ are the Compton projection, the weight, and the filter function at the i th energy window, respectively.

In order to derive the filter functions h_i , using the line spread functions as good approximations of the system transfer functions, it is assumed that

$$\text{LSF}_S = \text{LSF}_i \bullet h_i, \quad (6)$$

where LSF_S and LSF_i are the LSF of the Compton component at the photopeak and at the i th energy window.

Using the Fourier theorem and indicating with F and F^{-1} the Fourier and Inverse Fourier transforms, respectively,

$$F(\text{LSF}_S) = F(\text{LSF}_i) \cdot F(h_i), \quad (7)$$

and the filter can be derived as

$$h_i = F^{-1} \left\{ \left[\frac{F(\text{LSF}_S)}{F(\text{LSF}_i)} \right] \cdot W \right\}, \quad (8)$$

where W is a window used to stabilize h_i (9).

The scatter corrected projections, $T(x, \Phi)$, are obtained by

subtracting the calculated scatter component, $S(x, \Phi)$, from the photopeak projections, $P(x, \Phi)$

$$T(x, \Phi) = P(x, \Phi) - S(x, \Phi). \quad (9)$$

In order to make this technique applicable in a clinical environment, a restriction of this general formulation was used and a single secondary Compton window was employed. Considering that scatter distribution would change moving the energy window far from the photopeak, the Compton energy window was set close to the photopeak, at 108–132 keV (120 keV, 20%).

Theoretical Considerations

The three scatter correction techniques can be described in a common general formulation based on two principal assumptions:

1. Measured data within the photopeak window (P) are the sum of true photopeak data (T) and scattered data (S)

$$P = T + S. \quad (10)$$

2. Scatter contribution S is not experimentally measurable, but can be expressed as

$$S = K \cdot Q \bullet f, \quad (11)$$

where Q are some kind of measurable data (photopeak, scatter, photopeak + scatter in the photopeak or in a Compton energy window), K is a scatter coefficient normalizing S to Q , and f is a filter function shaped in order to match S and Q in terms of system response function.

The three scatter correction techniques are different in the definition of Q and the assumptions needed to calculate f and K .

Let Q be the measured photopeak + scatter projections (P), $K = 1$, and f be an exponential function. Then

$$S = P \bullet f. \quad (12)$$

This is the convolution subtraction method approach.

Let Q be scattered data recorded within a secondary Compton window (C) and let us suppose the scatter distribution in the secondary window to be a good approximation of scatter distribution in the photopeak window, that is let f be a δ function. Then

$$S = K \cdot C \bullet \delta = K \cdot C. \quad (13)$$

Equation (13) is the "projection version" of equation (3) in the dual energy window method.

Finally let Q be scattered data within a secondary Compton window (C). Then

$$S = K \cdot C \bullet f, \quad (14)$$

which corresponds to equation (5) in the multi-energy window—filtering method.

It is interesting to note that another scatter correction technique, the deconvolution method proposed by Floyd et al. (5), can be described with this general formulation. If Q is assumed to be T , the true photopeak data in the photopeak energy window, and $K = 1$, then

$$S = T \bullet f, \quad (15)$$

which is in fact the assumption of the deconvolution scatter correction method.

TABLE 1
Subtraction Coefficients for the Multiple Energy Window Methods (Monte Carlo Simulations: Water Phantoms)

Phantoms	$K_J = \frac{\text{Scatter component (126-154 keV)}}{\text{(92-125 keV)}}$	$K_T = \frac{\text{Scatter component (126-154 keV)}}{\text{(108-132 keV)}}$
Line source $l = 7$ cm Cylinder $D = 20$ cm $h = 7$ cm	0.64	0.66
Extended source Cylinder $D = 20$ cm $h = 10$ cm Hot lesion $D = 4$ cm	0.54	0.57
Extended source Cylinder $D = 20$ cm $h = 10$ cm Cold lesion $D = 4$ cm	0.49	0.53
Extended source Cylinder $D = 20$ cm $h = 10$ cm	0.44	0.48

Monte Carlo Program

Monte Carlo programs permit the simulation through computer calculations of the complete process of gamma radiation detection with a gamma camera (SPECT system) (10-12). With a Monte Carlo program it is possible to follow the history of each gamma ray, step by step, from the emission point in the radioactive source up to the detection point in the NaI crystal until complete absorption or escape. It is thus possible to analyze simulated data in terms of energy and spatial distribution, discriminating scattered from nonscattered events, and, consequently, separating scatter from the non-scatter contribution (which in general is not possible in experimental situations).

The Monte Carlo program used allowed radioactive sources (phantoms), gamma camera collimator, and detector to be simulated.

Cylindrical and spherical water phantoms were simulated, representing the head and containing point, line, or distributed ^{99m}Tc (140 keV) radioactive sources. The shape and sizes of some of these phantoms are described in the first column of Table 1. Simulating the transport of photons inside the phantoms, photoelectric and Compton effects were taken into account. Due to the low energy of the ^{99m}Tc radiations, pair production was not considered.

The simulated collimator was a standard lead hexagonal parallel-hole (low-energy general-purpose) collimator with the same physical parameters as that used in experimental studies. Simulating the interaction of radiations in the collimator, photoelectric effect, Compton effect, and Rayleigh effect were considered.

The detector simulated was a NaI crystal ($D = 40$ cm, $h = 1.25$ cm). Photoelectric and Compton effects were included. X-rays production in the crystal was also considered.

A comparison between Monte Carlo simulated and experimental energy spectra of a line source in a water filled cylinder is shown in Figure 1. A good matching between the two spectra is found in the photopeak energy range and in most parts of the Compton spectrum. The disagreement between curves around 70-100 keV is due to the x-rays production in

the collimator which was not simulated (lead x rays: 73-87 keV). An overestimation of the Compton component in the experimental spectrum could also occur due to events scattered outside the detector and the phantom. The percent counts difference between the two spectra in the photopeak (126-154 keV), the 92-125 keV and the 108-132 keV energy windows was 2%, 10%, and 5%, respectively.

SPECT Detection System

The tomographic detection system consisted of a rotating gamma camera (General Electric 400AC) equipped with a low energy general purpose collimator and connected to a dedicated computer (Hewlett Packard 1000F). The reconstruction algorithm was a filtered back-projection algorithm, using a

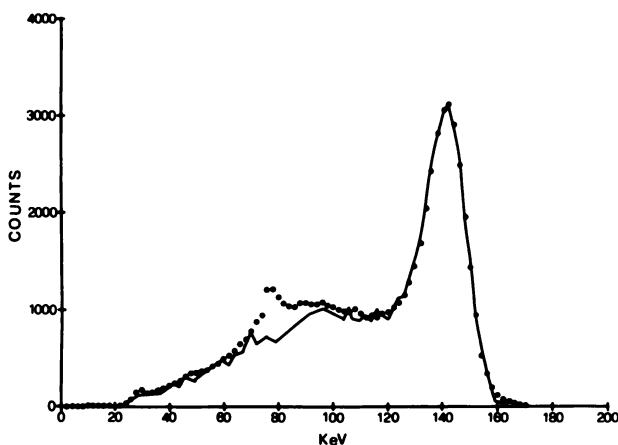


FIGURE 1
Comparison between Monte Carlo simulated (continuous line) and experimental (dotted line) energy spectra: ^{99m}Tc line source in a Plexiglas cylinder ($D = 20$ cm, $h = 7$ cm). The disagreement in part of the Compton spectrum is due to the x-rays production in the collimator which was not simulated and to a possible overestimation of the Compton component of the experimental spectrum from events scattered outside the crystal and the phantom.

generalized Hanning filter with a cut-off frequency of 0.5 pixel⁻¹. The algorithm included attenuation corrected by the Bellini method (13).

Assessment of Scatter Correction Method

Convolution subtraction method. In order to assess the spatial stability of the exponential filter, the parameters A and B were measured for two different experimental geometries and at different positions with respect to the center of rotation.

A line source ($D = 1$ mm, 7 cm long) was positioned within a Plexiglas cylinder and within a water filled elliptical phantom (described in the following), respectively, from 0 to 8 cm (for the cylinder) and from 0 to 10 cm (for the ellipse) from the phantom center, coincident with the center of rotation of the SPECT detection system (15 cm radius of rotation). For each source position, two opposing planar views (128×128 matrix size) were acquired at 0° and 180°, and the geometric means of the images were calculated. Line spread functions were then obtained. The scatter distribution function was defined from the tails of the LSF. The parameter A was calculated as "the ratio between the number of counts/channel at the intersection of the two slopes defining the scatter distribution and the total number of counts in the measured LSF" [see Axelsson (1)]. The parameter B was calculated as the slope of the scatter function itself (pixel⁻¹). Figure 2 shows A and B values for the two different experimental geometries (cylindrical and elliptical phantom) as a function of distance from the center. Even using the geometric mean of opposing views, it may be seen that A and B are not invariant within the object plane. Mean values were thus calculated and used for scatter correction.

Dual-Energy Window Method. The subtraction coefficient K_j is defined as the ratio between the scatter component within the photopeak energy window and the total counts recorded within the Compton secondary energy window. The first term cannot be directly measured from experimental data

and the Monte Carlo program was therefore used. This program allowed different source geometries to be simulated and the corresponding values of K_j to be calculated. In Table 1 some source/matter simulated distributions are listed with the corresponding K_j values.

Multi-energy window-filtering method. The subtraction coefficients K_T were calculated from Monte Carlo simulations as for K_j . For this method the total counts recorded within the 108–132 keV window was obtained and used for computation (Table 1).

The filter $h(x)$ for the 108–132 keV energy window was calculated from the Monte Carlo simulation of a line source ($D=1$ mm, $l=7$ cm) in a water filled cylinder ($D=20$ cm, $h=7$ cm). The Monte Carlo program provided images of the source corresponding to photons detected within the Compton (108–132 keV) and photopeak (126–154 keV) energy window, distinguishing, in this last case, between the scattered and nonscattered photons. Line spread functions were calculated from images corresponding to the Compton window and the scatter component in the photopeak window. The filter h_i was obtained as defined in Eq 8.

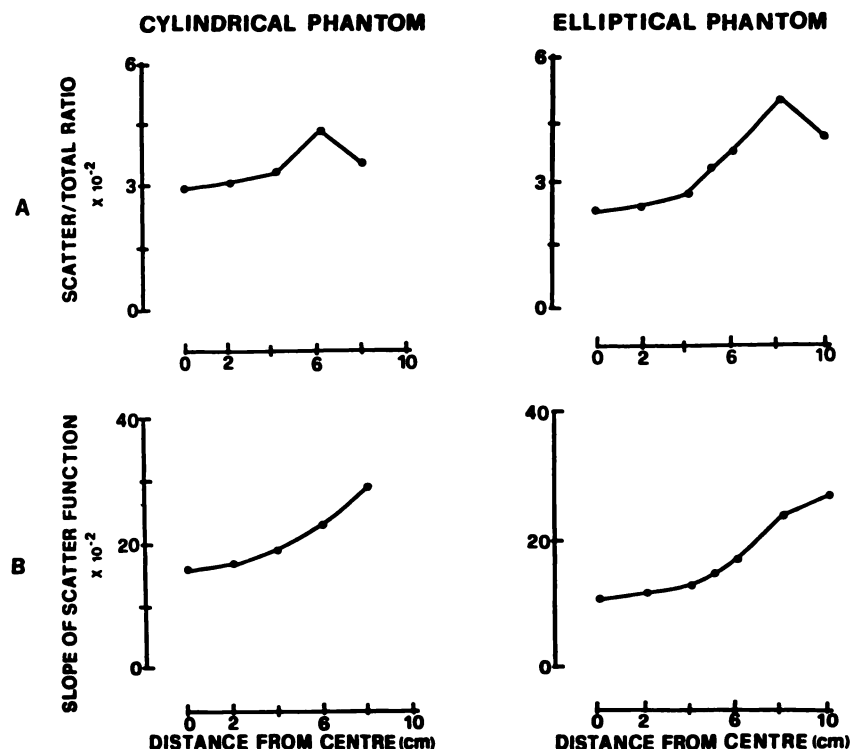
In Figure 3, the LSF for scattered photons within the photopeak energy window (126–154 keV) is compared with the LSF for the secondary Compton window (108–132 keV), before filtering (on the left) and after filtering (on the right). The better match of the curves after filtering demonstrates the efficacy of the filtering procedure.

SPECT Experimental Studies

In order to test the scatter correction algorithms for various source/matter distributions, several SPECT experimental studies were performed using different phantoms.

1. A line source ($D=1$ mm, $l=7$ cm) in air and scattering medium (Plexiglas cylinder $D=20$ cm, $h=7$ cm), positioned at 0,2,4,6 cm from the center of rotation.

FIGURE 2
Convolution subtraction method: values of A (top) and B (bottom) for a ^{99m}Tc line source in a Plexiglas cylinder (left) and a water filled elliptical phantom (right), as a function of the distance from the center.



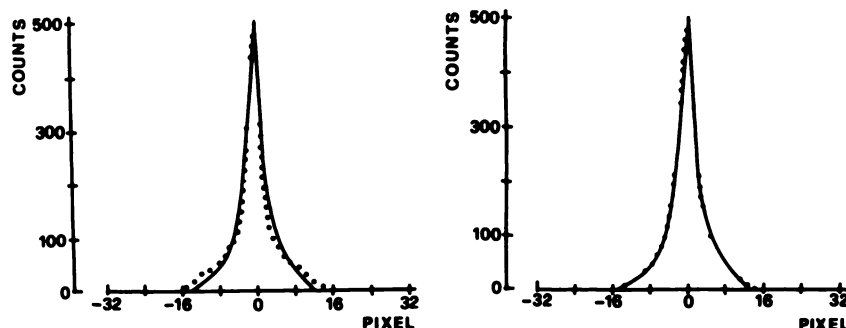


FIGURE 3
Multi-energy window-filtering method: comparison between LSF before filtering (left) and after filtering (right) from scattered photons within the photopeak energy window (126–154 keV) (continuous line) and within the secondary Compton window (108–132 keV) (dotted line).

2. A cold lesion phantom, consisting of a water filled cylinder ($D=20$ cm, $h=15$ cm) with Plexiglas rods ($D=3, 2.5, 2, 1.5, 1, 0.75, 0.5$ cm) parallel to the axis of the cylinder.

3. An elliptical phantom ($a=14$ cm, $b=22$ cm, $h=12$ cm); the bottom plate of the phantom is provided with a grid of holes where inserts different in shape and size can be positioned. Two cylindrical inserts ($D=4$ cm) filled with water were fixed inside the phantom, the background being radioactive (cold lesion study). A second set of measurements was performed using the same two cylinders, filled with radioactive solution, with a lesion/background radioactivity concentration ratio of 4:1 and 2:1, respectively, (hot lesion study).

Phantoms, filled with a uniform solution of ^{99m}Tc , were all positioned with the longitudinal axis coincident with the axis of rotation and, in order to avoid scatter and attenuation effects resulting from the bed, they were fixed to a holder, without any absorbing material between the source and the detector at any angular position. The radius of rotation was fixed at 15 cm. Sixty-four projections acquired over 360° were recorded for each SPECT study, each projection consisting of a 128×128 matrix for the line source studies, and a 64×64 matrix in all other studies. The count rate was always under 10,000 cps. Three scans were performed for each phantom study, using three different energy windows of 126–154 keV, 92–125 keV, 108–132 keV. Data were corrected for decay with respect to the starting time of the first scan and were then reconstructed without scatter correction and with scatter correction using the three techniques described above. Average scatter coefficients and parameters used for the different phantoms are reported in Table 2. Total counts in reconstructed photopeak images were ~ 0.8 million for the line sources and over 4 million for the other phantom studies.

Data Analysis

Quantitative accuracy. Total counts in the tomograms of the line sources in scattering medium were compared, with and without scatter correction, to total counts in the tomo-

grams of the line sources in air (no scatter and no attenuation), assumed as a reference.

Spatial resolution. Spatial resolution was measured in terms of full width at $1/2$, $1/10$, $1/30$ of the maximum of the LSF measured from counts profiles of the line sources in air and scattering medium without scatter correction and with scatter correction by the three methods described, at different positions of the source with respect to the center.

Contrast. Contrast was calculated for cold lesions both from the cold lesion phantom and the elliptical phantom studies. The minimum value of counts in each lesion (min) was determined and an average value of the active background around the cold lesions was calculated from 3×3 pixels large regions of interest (ROIs) (B, counts/pixel). Contrast was defined for each lesion as

$$C = \frac{B - \min}{B + \min} \quad (16)$$

The 3 cm lesion of the cold lesion phantom was excluded from contrast calculations, since, as a result of its central position in the phantom, it was too sensitive to gamma camera nonuniformity artifacts.

Signal/noise ratio. Signal/noise ratio (contrast/noise) was calculated for the cold lesions studies with and without scatter correction. It was defined as the net signal ($|$ lesion-background count density $|$) divided by the standard deviation of the background count density. Average lesion count density was calculated from ROIs, 3×3 pixels large. Background average counts density and standard deviation were calculated from ROIs 3×3 pixels large, drawn around the lesions. Image counts in the cold lesions phantom study were 5.8 million with and 7.6 million without scatter correction, respectively. For the elliptical phantom cold lesion study, counts were 3 million and 4.5 million, respectively.

Recovery. Recovery, defined as the measured lesion to background count ratio divided by the true ratio (14), was

TABLE 2
Scatter Coefficients and Parameters Used for Scatter Correction

Phantoms	Convolution subtraction method		Dual-energy window method	Multi-energy window filtering method
	A	B(pixel $^{-1}$)	K_L	K_T
Line source	0.032	0.2	0.64	0.66
Cold lesion cylindrical phantom	0.032	0.2	0.53	0.56
Head elliptical phantom	0.030	0.15	0.53	0.56

calculated for all hot lesions. Regions of interest (3×3 pixels large) were drawn on hot lesions and background in order to obtain average counts/pixels values. The expected (true) ratio was measured by counting samples of the lesions and background radioactive solutions with a NaI spectroscopy system, after the SPECT study.

RESULTS

Scatter Component

Images of scatter distribution within the photopeak energy window, as evaluated with the three techniques, are presented in Figure 4 for the hot lesion elliptical phantom study. The scatter component in terms of total counts was very similar for the three methods. However, while the scatter distribution for the convolution subtraction method is fairly uniform, for the two dual-energy window methods, a more shaped distribution, similar to the photopeak radioactivity distribution, can be observed.

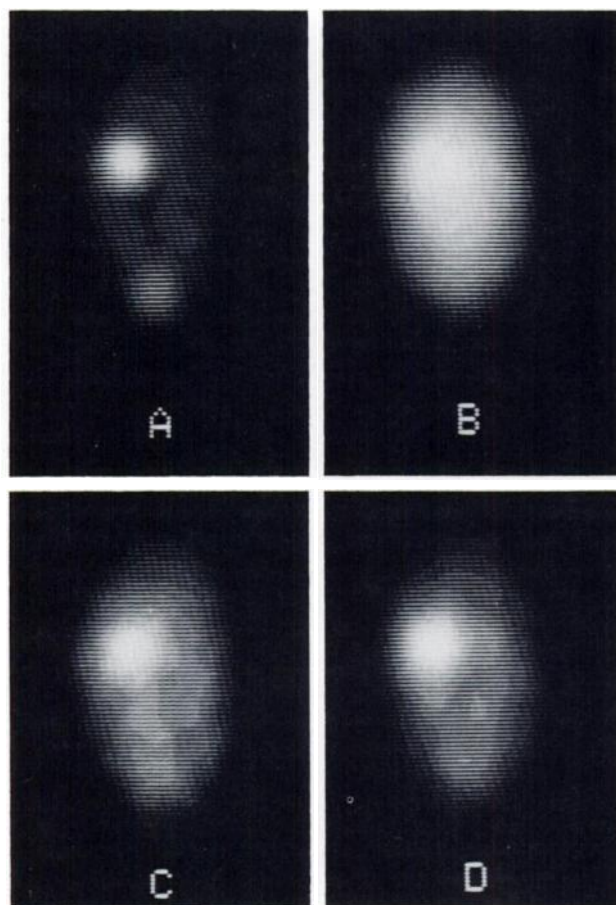


FIGURE 4

Hot lesion study: photopeak image without scatter correction (A), scatter component as evaluated by the convolution subtraction method (B), the dual-energy window method (C), the multi-energy window-filtering method (D).

TABLE 3
Comparison of Total Counts in Air and Scattering Medium (% Difference) for ^{99m}Tc

R (cm)	No scatter correction	Convolution subtraction method	Dual-energy window method	Multi-energy window-filtering method
0	+26.5	+0.6	+2.4	+4.9
2	+29.9	+1.7	+2.7	+4.8
4	+32.1	+5.9	+4.1	+6.9
6	+26.5	+7.8	+3.1	+6.6

R = Source-Center distance.

Quantitative Accuracy

Percent differences of total counts in the tomograms of the line source in scattering medium without scatter correction and after scatter corrections with respect to total counts in the tomograms of the line sources in air are shown in Table 3. If no scatter correction is applied, an overestimation in counts of about 30% was found. All three scatter compensations improve this quantitative accuracy. With the equipment used for these tests, there was an unexplained edge effect for data within 2 cm of the surface of the phantom.

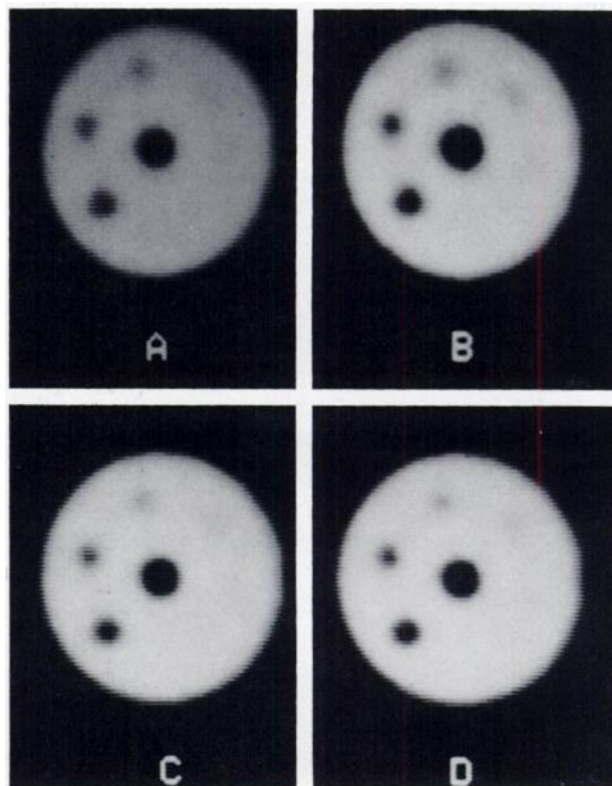


FIGURE 5

Cold lesion study: without scatter correction (A), with scatter correction by the convolution subtraction method (B), the dual-energy window method (C), the multi-energy window-filtering method (D).

Spatial Resolution

The comparison of LSF of line sources in scattering medium without and with scatter correction showed a slight improvement in spatial resolution for all the methods, the reduction of the full width at $\frac{1}{2}$, $\frac{1}{10}$, $\frac{1}{30}$ of maximum observed being of the order of 2%, 4%, 8%, respectively. The agreement between spatial resolution values after scatter correction and in air was better than 2%.

Contrast

Images of the cold lesion phantom study are presented in Figure 5, before and after scatter correction. A significant increase in cold lesion contrast was observed for various lesions size, being ~40% for all three methods (Fig. 6). The expected contrast value of 100% is approached only for the largest lesion ($D = 4$ cm) where spatial resolution does not affect contrast measurement. In Figure 7 profiles through a cold lesion in the elliptical phantom study before and after scatter correction are compared.

Signal/Noise Ratio

Values of signal/noise ratio (contrast/noise) are reported in Table 4. An increase in signal/noise ratio was observed after scatter corrections. This results from the gain in signal (contrast) being much greater than the increase of noise, resulting from the correction process. This indicates the usefulness of the scatter correction method.

Recovery

Results giving the recovery coefficient for two hot lesion studies, using the elliptical phantom, are summarized in Table 5 for two lesion/background radio-

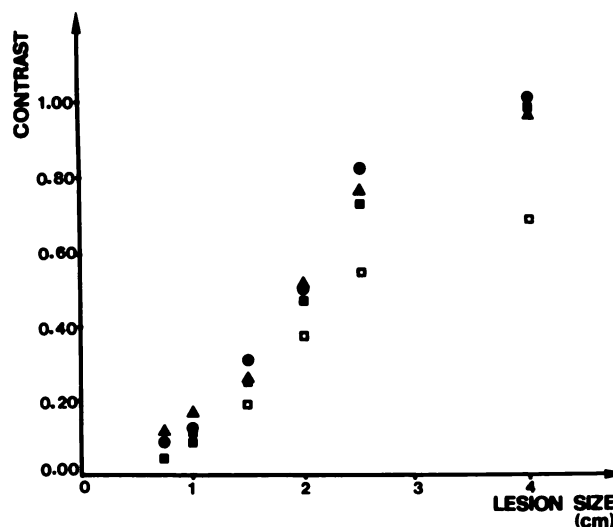


FIGURE 6

Cold lesion study: contrast values vs. lesion size. (□) without scatter correction; (●) convolution subtraction method; (■) dual-energy window method; and (▲) multi-energy window-filtering method.

activity concentration ratios. Recovery, as contrast, was significantly increased after scatter corrections (~20%) for all three scatter compensation techniques.

DISCUSSION

Radiation scatter is an object-dependent phenomenon; an ideal scatter compensation technique should account for the spatial nonstationarity of the scatter

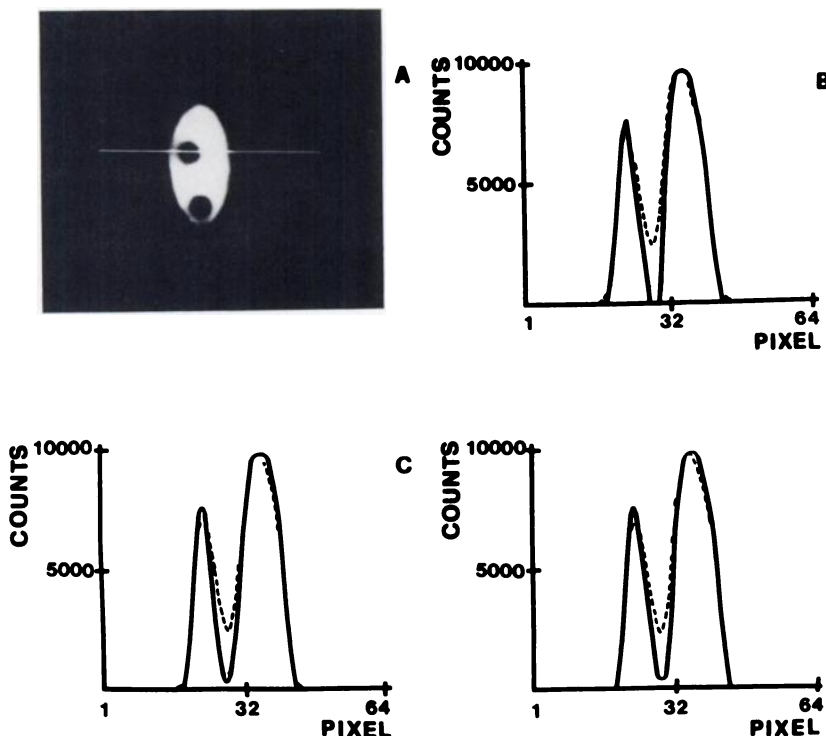


FIGURE 7

Cold lesion study: image of the photopick radioactivity distribution (A); comparison between profiles through the cold lesion without scatter correction (dotted line) and after scatter correction (continuous line) by the convolution subtraction method (B); the dual-energy window method (C); and the multi-energy window-filtering method (D).

TABLE 4
Signal/Noise Ratio

	No scatter D' (cm) correction	Convolution subtraction method	Dual-energy window method	Multi-energy window-filtering method
4.00	19.4	27.5	28.7	26.4
2.50	19.6	25.2	21.0	22.3
2.00	14.4	19.8	19.5	15.9
1.50	8.8	11.3	9.6	10.9
1.00	3.7	5.2	4.3	5.2
0.75	—	3.8	3.3	3.6
0.50	—	—	—	—

* Lesion diameter.

distribution, and the dependence of the scatter component upon experimental geometry, source, and matter distribution. Blurring due to scatter can be reduced by simple methods of image manipulation, such as by performing a uniform background subtraction. Such methods may improve image contrast, but are not adequate to obtain quantitative data, in terms of absolute radioactivity concentration (4), nor do they change signal/noise ratio.

The aim of the present work was to unify the mathematical description and to assess comparatively presently available techniques, potentially useful for quantitative scatter correction procedures. Three scatter compensation techniques have been considered, all based on the estimate of the true scatter component within the photopeak energy window: a single-energy window method (convolution subtraction method), and two multiple energy window methods (dual-energy window and multi-energy window — filtering methods). As the assumptions made for calculating the scatter component of recorded data are different, different experimental procedures and data processing techniques have to be used for each method. Thus, calibration of each method was performed by determining, for each SPECT study, the most appropriate scatter coefficients and weighting factors, taking the shape of the phantom and the distribution of radioactivity into account. In particular, the convolution subtraction method and the multi-energy window — filtering method include a filtering procedure, and the shape of the filter function changes in the image plane and depends on the source geometry. The hypothesis of stationarity was adopted and average coefficients were therefore calculated for the first technique, while, for the last method, a constant filter was assumed, as calculated from the simulation of a line source in the center of a cylindrical water phantom. On the other hand, the multiple energy window methods, because scatter distribution is experimentally measured within the secondary energy window, include information about the spatial variation of scatter.

TABLE 5
Hot Lesion Recovery

	No scatter Q' correction	Convolution subtraction method	Dual-energy window method	Multi-energy window-filtering method
2:1	0.76	0.92	0.90	0.89
4:1	0.71	0.88	0.90	0.84

* Lesion to background radioactivity concentration ratio (lesion diameter = 3.5 cm).

Once calibrated, the three scatter correction methods have been applied to SPECT phantom studies. The spatial distribution of scattered events was found to be shaped in a way similar to the photopeak radioactivity distribution when measured with the multiple energy windows methods, and it appeared to be more uniform, but still shaped, when calculated by the convolution subtraction method (Fig. 4). After scatter correction a significant improvement in image quality and quantitative accuracy (in particular in terms of image contrast and recovery) was found, confirming the importance of scatter correction in SPECT and demonstrating the efficacy of the three methods considered.

The lack of significant differences in performance among the three techniques, in spite of the different estimated scatter distributions, can be primarily explained by the physical limitations of the SPECT technique itself and the nonstationary nature of these correction methods. The poor spatial resolution of the system does not allow an accurate definition of structures and radioactivity distribution in the object. However, in addition, the data analysis technique used is not particularly sensitive to the variations in regional radioactivity distribution. Results were expressed as "global" parameters (contrast, signal/noise ratio, recovery), estimated by average counts/pixel evaluations and therefore were not strongly affected by local variations of radioactivity distribution.

Limitations in the accuracy of estimating the scatter component are still present in the methods and might also explain why no one technique is really superior to the others. In particular, possible sources of error in the evaluation of the Compton component are:

1. Limitations in the accuracy of the simulation technique (phantom measurements or computer codes, such as Monte Carlo programs) used in order to calculate the coefficients, characteristic of each scatter correction method.
2. The unwarranted assumption that the scatter distribution within a secondary energy window is a good estimate of the true scatter distribution within the photopeak energy window, as in the dual-energy window method, disregarding the different response function of the system at different energy windows.

3. The use of spatially invariant coefficients, averaged on the image plane, as in the convolution subtraction method, or estimated as constrained approximation of the real measurement conditions, as in the multi-energy window — filtering method (stationary techniques, in their present form).

4. The monodimensional nature of the filtering procedures, implicit in the correction technique applied within a slice. An extension into three-dimensional space (3-D) should be performed by the definition of bidimensional (2-D) filters. In fact in the convolution subtraction method, an equivalent convolving filter has been proposed in 3-D (15), which should provide slightly better results than in 2-D. Bidimensional filters on the projections should be used in the multi-energy window — filtering method, replacing monodimensional filters applied to the sinograms.

Several factors other than scatter introduce errors in SPECT data. The variation of the collimator response function as a function of distance introduces object-independent, but nonstationary effects. Radiation attenuation, as well as scatter, is object-dependent and nonstationary. Correction procedures taking these effects into account have to be considered. Simultaneous correction for scatter, attenuation, and collimator function have been incorporated in a unified tomographic reconstruction algorithm based on an inverse Monte Carlo technique and using an iterative Maximum Likelihood estimator (7). The drawback of this method, even providing accurate data, is the long computing time. More recently, a method for the elimination of nonstationary effects as part of attenuation, scatter, and point spread function correction has been presented (16).

In summary, scatter correction improves image quality and quantitation accuracy. Notwithstanding methodologic limitations, the results obtained are encouraging, thus suggesting the usefulness of scatter correction procedures on clinical images.

REFERENCES

1. Axelsson B, Msaki P, Israelsson A. Subtraction of Compton-scattered photons in single-photon emission computerized tomography. *J Nucl Med* 1984; 25:490–494.
2. Jaszczak RJ, Greer KL, Floyd CE, et al. Improved SPECT quantification using compensation for scattered photons. *J Nucl Med* 1984; 25:893–900.
3. Todd-Pokropek AE, Clarke G, Marsh R. Preprocessing of SPECT data as a precursor for attenuation correction. In: Deconinck F, ed. *Information Processing in medical imaging*. Bruxelles: Martinus Nijhoff Publishers, 1983:130–150.
4. Jaszczak RJ, Floyd CE, Coleman RE. Scatter compensation techniques for SPECT. *IEEE Trans Nucl Sci* 1985; NS32:786–793.
5. Floyd CE, Jaszczak RJ, Greer KL, et al. Deconvolution of Compton scatter in SPECT. *J Nucl Med* 1985; 26:403–408.
6. Oppenheim BE. Scatter correction for SPECT. *J Nucl Med* 1984; 25:928–929.
7. Floyd CE, Jaszczak RJ, Coleman RE. Inverse Monte Carlo: a unified reconstruction algorithm for SPECT. *IEEE Trans Nucl Sci* 1985; NS32:779–785.
8. Egbert SD, May RS. An integral-transport method for Compton—scatter correction in emission computed tomography. *IEEE Trans Nucl Sci* 1980; NS27:543–547.
9. Marsh R. Scatter correction for single photon emission computed tomography images. Thesis. University College London, London, UK, 1983.
10. Floyd CE, Jaszczak RJ, Harris CC, et al. Energy and spatial distribution of multiple order Compton scatter in SPECT: a Monte Carlo investigation. *Phys Med Biol* 1984; 29:1217–1230.
11. Floyd CE, Jaszczak RJ, Harris CC, et al. Monte Carlo evaluation of scatter subtraction in single photon emission computed tomography. *Med Phys* 1985; 12:776–778.
12. Manglos SH, Floyd CE, Jaszczak RJ, et al. Experimentally measured scatter fractions and energy spectra as a test of Monte Carlo simulations. *Phys Med Biol* 1987; 32:335–343.
13. Bellini S, Piacentini M, Cafforio C, et al. Compensation of tissue absorption in emission tomography. *IEEE Trans* 1979; 3(ASSP-27):213–218.
14. Hoffman EJ, Huang SC, Phelps ME. Quantitation in positron emission computed tomography: 1. Effect of object size. *J Comput Assist Tomogr* 1979; 3:299–308.
15. Larsson SA, Axelsson B, Dahl CM, et al. The use of 1-D and 2-D scatter correction techniques for contrast enhancement and quantification in SPECT. *J Nucl Med* 1986; 27:P884.
16. Todd-Pokropek AE. The elimination of nonstationary effects as part of attenuation, scatter, and PSF correction in tomography. *J Nucl Med* 1987; 28:660–661.